the plant journal

Plastidial ACP Δ9-desaturase controls EPA biosynthesis and TAG accumulation in *Phaeodactylum tricornutum*

Journal:	*The Plant Journal*
Manuscript ID	TPJ-01104-2020
Manuscript Type:	Original Article
Biochemistry and Physiology:	Fatty acid metabolism < Lipid metabolism, Metabolic engineering, Membranes < Lipid metabolism, Other (please specify) < Lipid metabolism
Cell Biology:	
Genomics & Genetics:	
Plant Growth & Development:	
Plant interactions with other organisms:	
Plant Responses to Environment:	
Other (please specify):	Diatoms, Triacylglycerol synthesis

Plastidial ACP Δ9-desaturase controls EPA biosynthesis and TAG accumulation in *Phaeodactylum tricornutum*

Richard Smith[a,1], Juliette Jouhet[b], Chiara Gandini[a, 2], Vladimir Nekrasov[a], Eric Marechal[b], Johnathan A. Napier[a*], Olga Sayanova[a*]

[a] Department of Plant Sciences, Rothamsted Research, Harpenden, Herts, AL5 2JQ UK;

[b] Laboratoire de Physiologie Cellulaire et Végétale Univ. Grenoble Alpes, CNRS, IRAE, CEA, IRIG, 38000, Grenoble, France

[1] Current address: Algenuity, Eden Laboratory, Broadmead Road, Stewartby, MK43 9ND, UK

[2] Current address: Open Bioeconomy Laboratory, Department of Chemical Engineering and Biotechnology, University of Cambridge, Cambridge CB3 0AS

* For correspondence: Olga Sayanova and Johnathan Napier

Email: olga.sayanova@rothamsted.ac.uk ; johnathan.napier@rothamsted.ac.uk

Keywords

Phaeodactylum tricornutum, Δ9-desaturase, eicosapentaenoic acid, lipids, omega-3 PUFA biosynthesis

Author Contributions

O.S., J.A.N. and V.N. designed research; R.S., J.J. and C.G performed research; R.S., J.J., E.M. and O.S. analysed the results. R.S., O.S. and J.A.N. wrote the paper.

Abstract

The unicellular marine diatom *Phaeodactylum tricornutum* accumulates up to 35% eicosapentaenoic acid (EPA, 20:5n3) and has been used as a model organism to study long chain polyunsaturated fatty acids (LC-PUFA) biosynthesis due to an excellent annotated genome sequence and established transformation system. In *P. tricornutum*, the majority of EPA accumulates in polar lipids, especially in galactolipids such as mono- and di-galactosyldiacylglycerol (MGDG and DGDG). LC-PUFA biosynthesis is considered to start from oleic acid (18:1n9). EPA can be synthesized via a series of desaturation and elongation steps occurring at the endoplasmic reticulum and newly synthesized EPA is then imported into the plastids for incorporation into galactolipids via an unknown route. The basis for the flux of EPA is fundamental to understanding LC-PUFA biosynthesis in diatoms. We used *P. tricornutum* to study acyl modifying activities, upstream of 18:1n9, on subsequent LC-PUFA biosynthesis. We identified the gene coding for the plastidial acyl carrier protein Δ9-desaturase, a key enzyme in fatty acid modification and analysed the impact of overexpression and knock out of this gene on glycerolipid metabolism. This revealed a previously unknown role of this soluble desaturase in EPA synthesis and production of TAG. This study provides further insight into the distinctive nature of lipid metabolism in the marine diatom *P. tricornutum* and suggests a new approach for tailoring oil composition in microalgae.

Significance Statement

In the marine diatom *Phaeodactylum tricornutum,* the main chloroplast lipids are enriched in eicosapentaenoic acid (EPA) despite its synthesis on the ER. We show that committed EPA biosynthesis commences with the action of a plastidial acyl carrier protein (ACP)-Δ9 desaturase, using palmitic acid (16:0) as substrate. Targeted mutagenesis of this gene leads to an EPA increase and decreased triacylglycerol (TAG), providing evidence that PAD acts as a regulating enzyme for EPA and TAG production.

Introduction

In recent years microalgae have attracted considerable attention as an alternative and sustainable platform to produce high value lipids. However, biotechnological improvement of algal strains requires further advances in our understanding of algal physiology and metabolic pathways, coupled with the refinement of molecular toolkits. Heterokonts represent a major group of microalgae containing more than 16.000 species and are major constituents of the collective biomass known as phytoplankton. Diatoms are thought to have derived from a secondary endosymbiotic event when a red alga was engulfed by a eukaryotic host cell. This led to the formation of secondary plastids surrounded by four membranes, corresponding to the exosymbiont endomembrane, the plasma membrane of the engulfed alga, and the two membranes of the primary plastids (1). It was demonstrated that in Heterokont species the outermost secondary chloroplast limiting membrane forms a continuum with the outer membrane of the endoplasmic reticulum (ER) (2). The chloroplast lipid profiles are characterized by the presence of four major lipid classes such as monogalactosyldiacylglycerol (MGDG), digalactosyldiacylglycerol (DGDG), sulfoquinovosyldiacylglycerol (SQDG) and phosphatidylglycerol (PG).

Recently, comprehensive studies of the glycerolipid content of two *Phaeodactylum tricornutum* ecotypes, Pt1 and Pt4, have demonstrated that the glycerolipid profiles are dominated by MGDG, SQDG, DGDG and phosphatidylcholine (PC) (~75% of the total content) while non-polar lipids, diacylglycerols (DAG) and triacylglycerol (TAG), represent ~ 3% of the total glycerolipids (3, 4). In many Heterokonts species, thylakoid lipids contain the long chain polyunsaturate, eicosapentaenoic acid (EPA, 20:5n3) (3, 5). EPA synthesis occurs in the ER (6), implying the existence of unknown pathway(s) for its trafficking from the ER into the chloroplast. The current understanding of lipid metabolism and fatty acid synthesis in algae is based on genomic analysis and metabolic models derived from higher plants. However, since higher plants neither contain EPA nor display the hallmarks of secondary endosymbionts, such parallels have their limitations. In terms of commonality, *de novo* FA synthesis in diatoms occurs in plastids and leads to formation of a C16-acyl carrier protein (ACP) by the fatty acid synthase of type II (FASII). In plants, the C16-ACP is then i) either retained in the plastids where it can be esterified by chloroplastic acyltransferase to glycerol-3-phosphate (G3P) for conversion into organellar membrane lipids (the so called “prokaryotic” pathway); ii) hydrolyzed from ACP by specific

fatty acyl-ACP thioesterases (FATs) that release free fatty acids (FFAs) in the inner envelope of the chloroplast or iii) further elongated to C18-ACP. Alternatively, 16:0- and 18:0-ACPs can undergo further desaturation by the soluble ACP desaturases of the chloroplast stroma (7) and subsequently released by FATs. So far, no FATs similar to that of plants and bacteria have been identified in diatoms (8). The formation of C16-18 FFA is considered the final step of *de novo* plastidial FA biosynthesis followed by the export of these fatty acids to the cytosol after being esterified to coenzyme A (CoA) by a long-chain acyl-CoA synthase (LACS) located in the outer envelope of the plastid to form acyl-CoAs (9, 10). These neosynthesized FAs may be further elongated or desaturated in the ER and used for glycerolipid synthesis (the so-called "eukaryotic pathway"). In plants, desaturation of 18:0 can be catalyzed either by the soluble stearoyl-ACP Δ9-desaturase (SAD) of the chloroplast stroma (7) or by an extra-plastidic ER-bound acyl-CoA Δ9-desaturase (ADS) (11), both generating 18:1n9, although SAD is the dominant pathway. Since only small amounts of C18-FAs could be detected in diatom chloroplast lipids, there is no direct evidence of 18:0-ACP synthesis in the plastids of diatoms, underlining another difference from plant FA biosynthesis. LC-PUFA biosynthesis is considered to start with desaturation of 18:1n9 by a Δ12-desaturase resulting in the production of linoleic acid (LA; 18:2n6) which is subsequently converted into α-linolenic (ALA; 18:3n3) by the action of Δ15-desaturase. Both LA and ALA are then converted into LC-PUFAs by the sequential desaturation/elongation reactions of that pathway.

The unicellular marine diatom *P. tricornutum* accumulates up to 35% of EPA and has been used as a model to study LC-PUFA biosynthesis due in part to a well-annotated genome sequence (12) and established transformation systems (13). In *P. tricornutum*, the majority of EPA accumulates in polar lipids, especially in galactolipids such as MGDG and DGDG (3, 14, 15). Pulse chase experiments in *P. tricornutum* revealed that EPA can apparently be synthesized by a number of different routes with the predominant pathway proceeding *via* Δ6-desaturation of LA and ALA, and utilizing intermediates of both n6- and n3-pathways (16). Two main classes of FA desaturases involved in LC-PUFA biosynthesis have been previously identified in *P. tricornutum* and functionally characterized in yeast. Firstly, soluble enzymes, exemplified by PtFAD6, adding a double bond to an acyl-ACP substrate and secondly transmembrane enzymes (such as PtFAD2, PtD6 and PtD5), adding a double bond on acyl-glycerolipid susbtrates (17, 18). Based on these observations, it was suggested that both Δ6- and Δ5- desaturation and Δ6-elongation take

place in the ER and newly synthesized EPA is then imported into the plastids for incorporation into galactolipids via an unknown route called the “omega pathway” (19). The understanding of EPA channelling is fundamental to manipulating LC-PUFA biosynthesis in diatoms.

To date, the mechanism of FA biosynthesis and export from the plastid in diatoms is still unknown. Since the 16:0 and 16:1n7 are the main FA synthesized in *P. tricornutum* chloroplast (3) it is possible that the *P. tricornutum* acyl-ACP desaturase might utilize only 16:0-ACP substrate, acting specifically as a palmitoyl-ACP desaturase (PAD) rather than a stearoyl-ACP desaturase (SAD). Since 18:1n9 is considered to be a precursor of LC-PUFA synthesis in the ER and cannot be derived from 16:1n7, acyl-ACP-Δ9 desaturase therefore represents an interesting target to modulate the accumulation of 18:0 and all downstream metabolites, including EPA. We overexpressed or disrupted the gene coding for the acyl-ACP-Δ9 desaturase and analysed the impact on glycerolipid metabolism, revealing an unexpected effect of this soluble plastidial desaturase on EPA synthesis in the ER and also production of TAG. Our results indicate that the omega pathway relies on channelling processes occurring very early in plastidial FA desaturation and that this process can also be considered as a rate-limiting step in TAG synthesis.

Results

Generation of transgenic *P. tricornutum* overexpressing an acyl-ACP Δ9-desaturase. Based on bioinformatic analysis only one homologue of the Arabidopsis soluble stearoyl-ACP Δ9-desaturase (SAD) gene, Phat3_J9316, can be found in the *P. tricornutum* genome (12, 20). It contains predicted N-terminal bipartite targeting sequences with the conserved amino acid sequence motif “ASAFAP” surrounding the signal peptide cleavage site in diatoms {Kilian, 2005 #1643} (*SI Appendix*, Fig. S1*A*), consistent with a stromal location.

The native Phat3_J9316 acyl-ACP Δ9-desaturase sequence was chemically synthesized (Genscript, USA) and cloned into pPhos2 vector (21) under control of the EF2 promoter (22). The resulted construct, pPhos2-PAD (*SI Appendix*, Fig. S1*B*) was used to transform *P. tricornutum* via particle bombardment. A total of 38 zeocin-resistant were screened by PCR for the presence of the transgene, out of which 20 were positive. The fatty acid analysis of all PCR positive transformants revealed that 14 transgenic cell lines

had elevated levels of 16:1n7 compared to that of wild type (WT) (*SI Appendix*, Fig. S2*A*). Analysis of transcript abundance of two representative lines (PtPAD#16 and PtPAD#32) with a clear chemotype of elevated 16:1n7, confirmed expression of the codon optimised gene and no change in endogenous gene expression (*SI Appendix*, Fig. S2*B*). Overexpression of the acyl-ACP Δ9-desaturase gene does not significantly change the total FA accumulation relative to WT, with an average total FA contents per cell of 3.2 nmol FA/million cells when harvested after 3 days of cultivation (*SI Appendix*, Fig. S2*C*).

Overexpression of acyl-ACP Δ9-desaturase in transgenic *P. tricornutum* results in reduced levels of EPA and alteration in lipid profiles. The fatty acid profiles of PAD#16 and PAD#32 were further analysed during the exponential (E) and stationary (S) phases of growth (Fig. 1*A*, *SI Appendix,* Fig. S3*A*). In accordance with previous observations (21), the major fatty acids in *P. tricornutum* Pt4 WT cells are palmitic acid (16:0), palmitoleic acid (16:1n7), and EPA. Transgenic lines overexpressing the acyl-ACP Δ9-desaturase accumulated significantly higher levels of 16:1n7 compared to that of WT at both growth stages. In the E phase the relative concentration of 16:1n7 is increased from 0.6 µg FA 10^6 cells ml^{-1} in the WT to 0.9-1.0 µg FA 10^6 cells ml^{-1} in the overexpression lines (1.5 fold, mean of both strains, $p<0.05$, Least Significant Different, LSD), (Fig. 1*A*) and remains elevated in both lines relative to the WT (1.4 -fold, $p<0.05$, LSD) at S stage (*SI Appendix,* Fig. S3*A*). In addition, the products of further desaturation of 16:1n7, following the route proposed by Domergue et al. (23), 16:1n7 → 16:2n4 → 16:3n4 → 16:4n1, and elongation to 18:1n7 also increased significantly ($p<0.05$, LSD) in E phase and remained elevated in S phase compared to the WT. An increase in 16:1n7 is correlated with a reduction in the substrate 16:0 (0.52 - fold in the E phase and 0.65- fold in the S phase, $p<0.05$, LSD).

Acyl-ACP Δ9-desaturase overexpression resulted in a significant decline of the FA intermediates involved in the proposed predominant route of LC- PUFA biosynthesis based on radiolabelling experiments (16): 18:1n9 →18:2n6 → 18:3n6→18:4n3. This was followed by the significant (~2- fold, $p<0.05$, LSD) reduction of the final products of the pathway, EPA (from 0.79 µg FA 10^6 cells ml^{-1} in the WT to an average of 0.36 µg FA 10^6 cells ml^{-1} in E growth phase (Fig. 1*A)* and from 0.5 to 0.25 to µg FA 10^6 cells ml^{-1} in S stage (*SI Appendix,* Fig. S3*A*) and DHA (from 0.08 to 0.04 µg FA 10^6 cells ml^{-1} in E growth and 0.04 to 0.02 µg FA 10^6 cells ml^{-1} in S growth stages). Together these data demonstrate an

important role that that acyl-ACP Δ9-desaturase plays in channelling substrates at the very earliest stage of PUFA biosynthesis.

In order to determine if overexpression of the Δ9-desaturase gene could alter FA composition and abundance of specific lipid classes, a comprehensive glycerolipidome analysis was carried out. Total lipids were extracted from cells in both the E and S phases. Firstly, the detection and positional distribution of lipid species were characterised using direct infusion tandem mass spectrometry (MS2) with preferential loss analysis after separation by 1D and 2D TLC (3). Subsequently, lipid classes and species were quantified from total lipid extracts using HPLC-MS/MS.

The glycerolipid profile of WT *P. tricornutum* Pt4 cells in E phase were largely made up of plastidial membrane lipids, MGDG (36.4%), SQDG (16.4%) and DGDG (9%) and extraplastidial lipid classes such as PC (10.7%), betaine lipid (BL) diacylglycerylhydroxymethyltrimethyl-β-alanine (DGTA, 8.9%) and TAG (7.4%) (Fig. 1*B*). In the WT cells grown to S phase, plastidial membrane lipids are degraded, resulting in a reduction in each class (MGDG, 0.39- fold; DGDG, 0.34- fold; SQDG 0.53 -fold; PG 0.06 - fold; relative to exponential phase) and TAG is increased 7-fold (*SI Appendix*, Fig. S3*B*). The glycerolipid profile of Pt4 contrasts with a recent analysis of Popko et al. (4), where major BL class was characterised by MS spectra as diacylglyceroltrimethyhomoserine (DGTS). Three main BLs have been identified in microalgae, DGTA, diacylglyceryl carboxyhydroxymethylcholine (DGCC) and DGTS. DGTA is a structural isomer of DGTS and the two molecules are difficult to differentiate by MS analysis alone. In this study, the presence of DGTA was confirmed by migration on 2D-TLC and M2S fragmentation (*SI Appendix,* Fig. S4). The presence and concentration of DGTA is similar to that reported in another *P. tricornutum* ecotype, Pt1 (3). We also confirmed the presence of EPA-acyl-SQDG, as reported previously, however this could not be quantified accurately by LC-MS/MS (3). The level of TAG in exponential phase of Pt4 was substantially higher (7.4%) than that reported in Pt1 (1-3%, (3), however it is important to note that the level of TAG is highly depended on growth conditions. Comparing the relative amounts of glycerolipids in acyl-ACP Δ9-desaturase over-expressers (OE), significant increase of MGDG was observed in the E stage of cell growth (1.34- fold, $p<0.05$ LSD), correlated with decrease in SQDG (0.73 fold), DGDG (0.78 fold) and DAG (0.71 fold) relative to WT ($p<0.05$ LSD) (Fig. 1*B*). There are no significant differences in proportions of lipid classes between WT and OE lines in the S phase (*SI Appendix*, Fig. S3*B*).

The *sn*-position of FAs on each glycerolipid was determined by preferential loss using MS and MS2 analysis as described in (24). In agreement with previous observations, EPA is overrepresented in membrane lipids ((3), (15); (25)). Considering chloroplast lipids, the major forms contain a C16 FA at the *sn*-2 position, suggesting that the prokaryotic pathway for the assembling of glycerolipids is very active in diatoms. The most abundant species in MGDG is 36:8, comprising of 20:5 and 16:3 (21%), whereas in DGDG dominant species are 20:5/16:2 (25.5%) and 20:5/16:1 (17.8%), and in PG, the major form is 20:5/16:1 (51%). (*SI Appendix,* Table S1). All these forms have a "prokaryotic" signature, a 20:5 at the *sn*-1 position and a C16 at the *sn*-2 position, supporting import of EPA into chloroplast from the ER, followed by plastidial acylation.

The overexpression of acyl-ACP Δ9-desaturase resulted in overall decline in all 20:5-containing species of chloroplast lipids (MGDG, DGDG, SQDG and PG) followed by an increase in C16-unsaturated containing species at both E and S stages of growth (*SI Appendix,* Tables S1- S4). We observed major reduction in the proportions of 20:5/16:3 form in MGDG (~ 4 -fold), 20:5/16:0 form in DGDG (~ 7-fold) and SQDG (4.8-6.8- fold) and 20-5/24:0 form in SQDG (12.6-fold) compared to WT. Extraplastidial polar lipids, PE, PC and DGTA, contain C16 FA together with C18, C20 and C22 FAs at *sn*-2 position, suggesting an unbiased FA species incorporation by microsomal acyl-CoA:lysophosphatidic acid acyltransferase (LPAAT) or the presence of acyl-CoA:lysophosphatidylcholine acyltransferase (LPCAT) that may synthesize the precursor backbones involved in ER membrane glycerolipid assembly. Noteworthy, 20:5 is present at *sn*-2 position only in the eukaryotic 20/20:5 form and 22:6 is found only in 20:5/22:6 form (*SI Appendix,* Tables S1- S4). In PE, *sn*-1 position was mainly occupied by 20:5 acyl group. In the overexpresors, the greatest reduction was observed in 20:5/C18- and 20:5/LC-PUFA- forms of PC, DGTA and PE with major decline of 20:5/20:5 form in PC and DGTA (~8.4-5 and 6.3-4.3-fold respectively) and 20:5/22:6 in PC (9.9-fold). The major alteration observed was an increase in 16:1/16:1 and 16:1/16:2 forms in PC (5.7-8.0 and 8.0-11.4- fold respectively, pmol 10^6 $cell^{-1}$) and DGTA (3.7-4.3 and 5.8-7.5-fold respectively, pmol 10^6 $cell^{-1}$). More surprising was an increase in 20:5 -16:1 and 20:5 -16:2 forms in PE (5.0-6.0- and 6.0-7.4-fold respectively, pmol 10^6 $cell^{-1}$) correlated with a decrease of these two major backbones in DGDG (~2 - 3-fold), suggesting that 20:5/16:1 and 20:5/16:2 species could be potentially exported as DAG.

Considering nonpolar lipids, the DAG pool is represented by 4 molecular species, comprising mainly of 16:1, 16:0 and 14:0 and 20:5 acyl groups, with 14:0 and 20:5 being found only at the *sn*-1 position. The DAG acyl composition (*SI Appendix,* Tables S1- S4) partially reflects that found in the main membrane lipids and we cannot rule out the recycling of the diacylglyceride backbone from membrane lipids. The major decline (~6-fold) has been observed in 20:5/16:0 form found in most polar lipids followed by an increase in 16:1/16:1.

Three DAG molecular species, 14:0/16:1, 16:1/16:1 and 20:5/16:0, are potential precursors of the TAG pool with *sn*-3 position occupied by 14:0 or C16 FA. In acyl-ACP Δ9-desaturase OE, TAG 20:5-containing species also declined followed by increase in 16:1 (*SI Appendix,* Tables S1-4). Similar FA backbone as in TAG, 20:5/16:0 with 20:5 FA at the *sn*-1 position was also reduced in direct precursor DAG and also in PC, DGDG and PG. The most significant alterations were observed in the increased proportions of 16:1/16:1- and decrease in 20:5/16:0- containing TAG species, suggesting that all these lipids may act as substrates for TAG biosynthesis.

Generation of transgenic *P. tricornutum* with acyl ACP Δ9-desaturase knocked out. To test the hypothesis that plastidial Δ9-desaturation of 16:0 within the chloroplast acts as a bottleneck for 16:0 export and further elongation and desaturation to EPA, the native Phat3_J9316 gene was targeted for disruption using CRISPR/Cas9 and two sgRNA guides to ensure gene disruption (Fig. 2*A, SI Appendix,* Fig. S5*A*). Cells were transformed using the previously described method (21) with the transformation efficiency ~ 1.6 colonies μg^{-1} plasmid. Among 33 colonies which were screened by PCR, two (Δ*pad*#3 and Δ*pad*#7) had a lower MW band, indicating deletion of sequences within the target gene (Fig. 2*B*). The sgRNAs were designed to generate a 57 nt deletion within the first exon of the gene (*SI Appendix,* Fig. S5*A*). Cloning and subsequent sequencing of the PCR products revealed mosaicism within each KO lines (*SI Appendix,* Fig. S5*B*-5*E*), including the insertion of a 371 bp fragment of the transformation vector backbone. The presence of bands >500 bp on the agarose gel in both lines indicates that larger insertions may also present in the cell population. The relative abundance of each deletion indicates that the deletion happened in multiple events after initial cell division. There was no detection of unaltered DNA sequence between the gRNAs in either

Δ*pad*#3 and Δ*pad*#7 lines, confirming a deletion in both these alleles. Consequently, the lines were analysed without further isolation of sub-clones. Both KO lines had significantly reduced levels of acyl-ACP Δ9-desaturase mRNA, most likely indicating increased post-transcriptional turnover of the mutated mRNA (Fig. 2*C*).

Fatty acid and glycerolipid analysis of transgenic *P. tricornutum* with disruption of endogenous acyl-ACP Δ9-desaturase reveals increases in EPA and major alterations in TAG. The fatty acid profiles of two disrupted/knock-out (KO) lines were analysed in the exponential and stationary phase of growth. KO of the acyl-ACP Δ9-desaturase gene resulted in a significant reduction of 16:1n7 (94% reduction relative to WT) and, consequently, in a smaller pool of products of further desaturation (16:2n4,16:3n4,16:4n1) and elongation (18:1n7) in both E and S phases (Fig. 3*A* and *SI Appendix,* Fig. S6*A*). In contrast, the accumulation of 16:0, a substrate for acyl-ACP Δ9-desaturase*,* increased ~1.45-fold followed by a significant increase in the levels of 18:1n9 vs WT, indicating independent desaturation of C18:0 by putative Δ9 acyl-CoA desaturase. Furthermore, the proportion of many intermediate FAs in extraplastidic PUFA synthesis pathway also significantly increased culminating in an elevated accumulation of EPA (~1.32-1.42-fold), increasing from 0.69 µg FA 10^6 cells^{-1} in the WT cultures, to 0.91-0.98 µg FA 10^6 cells^{-1} in the KO strains. Interestingly, the intermediates most affected by the KO (LA, ALA, 18:4n3, 20:4n3) are those highlighted by Arao and Yamada, 1994 to be involved in the dominant route of PUFA biosynthesis in *P. tricornutum* (16). The minor increase in proportions of DHA indicates that the pool size of EPA is not a bottleneck for synthesis; rather, as demonstrated by heterologous OtElo5 expression in *P. tricornutum*, accessibility of elongated products in the native strain is restrictive (21). The residual 16:1n7 found in the KO line profile may be produced in the cytosol by a homologue of Arabodopsis ADS1 (26) acting on 16:0-CoA and imported back into the plastid. We have identified only one candidate Δ9-oleyl CoA desaturase, PtADS1 (*Phatr3_J29797)* based on the sequence homology. Increased expression of a putative PtADS1 desaturase in KO lines relative to the WT (~2.4 fold) supports this hypothesis (Fig. 2*C*).

Glycerolipidomic analysis was carried out to determine how disruption of the acyl-ACP Δ9-desaturase gene affected the distribution of glycerolipids and FA within each class. The WT profile, sampled in E phase, was largely similar to the previously outlined

WT analysis, with the exception of a larger pool of TAG (24.5% vs 7.2% total lipid) which is likely due to slight differences in condition (synchronisation) of starting inoculum (Fig. 3*B*). Unlike the OE lines, KO of acyl-ACP Δ9-desaturase resulted in significant shift in the glycerolipid profile. KO lines had significant reduction in pools of MGDG (0.65-0.67-fold) and TAG (0.40-0.77-fold), and significant increases in SQDG (1.34-1.40-fold), PG (2.64-4.31-fold), PE (2.30-2.70-fold), PC (1.99-3.01-fold) and DGTA (1.65-3.26-fold). Lipid classes analysis (Tables S6-S10) reveal the major increase in "TAG-diagnostic" 20:5/16:0 species in main chloroplast lipids, SQDG (4.15-4.85-fold), MGDG (14.1-15.7-fold), DGDG (4.17-5.19-fold) and PG (3.76-7.01-fold) correlated with significant decrease in 16:1–containing species and metabolic derivatives (16:2, 16:3 and 16:4) were undetectable. A dramatic increase in C18-FA was observed in 20:5-containing lipids in MGDG and SQDG (~49-fold in 20:5/18:1 and 24-28-fold in 20:5/18:2 in MGDG; 3-5-fold increase in 20:5/18:2 in SQDG). The typical eukaryotic backbones, containing C18 FA and 20:4n3 at sn-2 position can come from the recycling of phospholipids such as PC, DGTA and PE similar to galactolipid synthesis in higher plants.

Within the extraplastidial PLs there was a major increase in unsaturated C18, 20:5 and 22:6 containing forms. The 20:5/20:5 form was slightly elevated in PE (1.5-fold), PC (1.8-fold) and DGTA (2-fold). Interestingly, an increase in 20:5/18:2 forms in PE, PC and DGTA was mirrored by similar changes in MGDG and SQDG, while 20:5/18:1 species concomitantly increased in PC, DGTA, MGDG and SQDG. This may imply that PE, PC and DGTA serve as precursors for galactolipids in *P. tricornutum*. The most significant changes in the DAG pool were increase in 20:5/16:0 form (21.65-22.92-fold) and disappearance of 16:1/16:1 (non-detected in KO strains). Alterations in TAG reflected that of membrane lipids and a DAG pool with a noticeable increase in 18:1 and 20:5-containing forms. Significant increase is detected in 20:5/16:0/16:0 (1.68-3.64-fold) and 20:5/20:5/16:0 (4.31-7.35-fold) forms.

Concerning changes in FA content, in chloroplast lipids in E phase of cell growth, EPA content increased significantly in SQDG (from 32.7 to 158.5 pmol FA 10^6 cells$^{-1,}$ ~5-fold) and in PG (3-5-fold) (Table S9) whereas in MGDG it remains unaltered. In extraplastidial lipids the most increase was observed in DAG (~11-fold) followed by significant increase in PE (1.9-2.2-fold) and PC (1.5-2.5-fold). A sharp increase in C18 FAs was detected in SQDG and MGDG, followed by a more moderate uptick in PE, PC and DGTA. 16:1 levels were markedly reduced in all lipids. Interestingly, the most

significant decrease in 16:1 was observed in DAG (26-72-fold), suggesting DAG pool is produced from neosynthesized FA. Similar pattern of FA accumulation was observed at S stage. In TAG, the most notable increase of EPA was observed in the stationary phase (~2-fold), followed by ~ 4-fold decrease in 16:1. Collectively, these observations support the hypothesis that the Phat3_J9316 acyl-ACP Δ9-desaturase acts as a competitor for 16:0 export and subsequent elongation/desaturation to EPA.

Heterologous characterization of the acyl-ACP Δ9-desaturase in *Synechocystis.* For the functional definition of the Phat3_J9316 acyl-ACP Δ9-desaturase activity evaluated above, the cyanobacteria *Synechocystis* PCC6803 strain was used as a heterologous expression system. The Δ9-desaturase sequence Phat3_J9316 lacking predicted signal peptide was cloned into the pUR expression vector and expressed in *Synechocystis* to confirm its enzymatic activity (*SI Appendix,* Fig. S7). *Synechocystis* has a relatively simple fatty acid profile with 16:0, 16:1n7, 18:0, 18:1n9, 18:2n6, 18:3n6 and 18:3n3 as the major fatty acids, whereas 18:4n3 and 18:1n7 are found only in trace amounts (*SI Appendix,* Fig. S8*A*). The expression of the Phat3_J9316 acyl-ACP Δ9-desaturase resulted in decreased levels of nearly all the major fatty acids except C18:0 and increased presence of C18 n7, the expected product of elongation of 16:1n7. To clarify the origin of 18:1n7, WT *Synechocystis* cultures were supplemented with 16:1n7 and grown until E phase before fatty acid analysis (*SI Appendix,* Fig. S8*B*). Exogenously supplied 16:1n7 only slightly increased the content of 16:1n7, but the levels of 18:1n7 were significantly increased, confirming the presence of a very efficient elongation of 16:1n7 to 18n7 in *Synechocystis* cells.

Altered Ultrastructure of Thylakoid membranes in transgenic *P. tricornutum* strains. Cross-sections of chloroplasts of E stage cells were analysed by transmission electron microscopy to access the impact of acyl-ACP Δ9-desaturase overexpression or inactivation on the ultrastructure of thylakoid membranes. WT chloroplasts contained several parallel thylakoid lamellae, each consisting of a stack of 3 membrane bilayers (*SI Appendix,* Fig. S9). Both mutants have disturbed thylakoid structure. The OE PAD#12 chloroplasts, containing more MGDG, has similar number of stacks, but they exhibit larger

luminal space with increased packing of stacks and more extreme curvature of the stacks (red arrow) and less parallelism between membranes is observed. In KO Δpad#3 chloroplasts, containing less MGDG, thylakoids are distorted, less electron dense than that of WT (blue arrow) with expanded inter-space, reduced stroma space and curvature of the lamella (green arrow), and no obvious pyrenoid is present.

Physiological studies. To explore whether the alterations of chloroplast ultrastructure have an impact on transgenic cells in different culture conditions, physiological studies were performed on the mutant and WT cells. Surprisingly, no differences were observed in specific growth rates and chlorophyll content between OE, KO and WT cells, suggesting that changes in thylakoid structure has no impact on the growth under normal conditions (*SI Appendix,* Fig. S10 and S11). To test the hypothesis that EPA acts as a sacrificial antioxidant molecule (to reduce ROX production under light stress), cellular growth of WT, OE PAD#16 and KO Δpad#3 strains was studied under light stress (*SI Appendix,* Fig. S12). Cultures were grown in 24 well plates under low light (20 µmol m^{-2} s^{-1}) for 2 days, then transferred to high light (250 µmol m^{-2} s^{-1}) and very high light (500 µmol m^{-2} s^{-1}) or maintained at low light. The OE PAD#16 strain (with reduced EPA synthesis) showed no difference compared to WT, whereas growth was perturbed in KO Δpad#3 after 4 days.

Discussion

Our study confirms that in the marine diatom *P. tricornutum* Pt4 the main FAs synthesized *de novo* in the stroma of chloroplasts are 14:0- and 16:0-ACP (3, 4)). We identified one sequence in *P. tricornutum* genome, Phat3_J9316, containing both a predicted signal peptide and chloroplast transit peptide with a diatom-specific ASAFAP motif, and orthologous to the Arabidopsis Δ9-stearoyl-ACP desaturase (SAD) gene. However, multiple lines of evidence support the classification of the Phat3_J9316 desaturase sequence as a Δ9 palmitoyl-ACP desaturase (PAD) as opposed to SAD. Firstly, the absence of 18:0 in *P. tricornutum* plastid lipids suggests that a soluble Δ9-acyl-ACP desaturase would act predominantly on 16:0-ACP, generating 16:1n7-ACP. Overexpression of Phat3_J9316 leads to an increase in 16:1n7 correlated with reduced levels of 16:0 and 18:1n9, indicating that the enzyme has a strong preference to 16:0 as

a substrate. In addition, we confirmed substrate specificity of Phat3_J9316 by functional characterization in the heterologous host *Synechocystis* providing evidence that increased accumulation of 18:1n7 in Phat3_J9316-overexpressing cells, is a result of ∆9-desaturase activity on 16:0 and the product of elongation of 16:1n7. In contrast, in *P. tricornutum* KO mutants, where Phat3_J9316 is disrupted by CRISPR-Cas9 gene-editing, there is a significant increase in levels of 16:0 consistent with the loss of PAD activity. Based on these results, we have assigned the function of palmitoyl-ACP ∆9-desaturase (PAD) to Phat3_J9316.

Overexpression of this PAD gene in *P. tricornutum* leads to an overall reduction of the FA intermediates (*SI Appendix,* Fig. S13). in the presumed predominant LC- PUFA biosynthetic pathway starting from 18:1n9 (16) and 2-fold decline in EPA and DHA, indicating that *PAD* plays a key role in channelling processes from the very early stage of PUFA biosynthesis and the desaturation of 16:0 in plastid likely to be a “crossroad” for acyl flux through to 20:5. This is supported by the enhanced accumulation of 20:5 and concomitant reduction in 16:1 in stationary phase TAGs of PAD KO cells (Fig. 4). Δ9-desaturation via PAD also regulates the levels of MGDG, the OE cells having higher MGDG levels while KO cells have lower, though both types of mutants displayed disturbed thylakoid membrane structures.

The inverse relationship between levels of 16:0/16:1 and EPA in OE and KO mutants, and the minor presence of C18 FA within chloroplast lipids, suggests that 16:0 is exported to the cytosol where it is converted into 16:0-CoA for further elongation and desaturation. This is in agreement with our previous observations that 20:5-CoA, 16:1-CoA and 16:0-CoA are the most abundant acyl-CoA species in *P. tricornutum* (21). Recently, Dolch et al., 2017 demonstrated that *Nannochloropsis gaditana* saturated fatty acid elongase, Δ0-ELO1, could elongate palmitic acid (27). *N. gaditana* Δ0-elo1 mutants exhibited a reduced EPA level and a specific decrease in MGDG. The study provided evidence that some of EPA used for MGDG production is biosynthesized by a channelled process initiated at the elongation step of palmitic acid by Δ0-ELO1, thus acting as a channelling enzyme for galactolipid production despite residing in the endoplasmic reticulum (27). We identified two putative saturated ER fatty acid elongases, Phatr3_J16376 (Δ0-Elo1) and Phatr3_J49867 (Δ0-Elo02), homologues of *N. gaditana* ER palmitic acid elongase Δ0-ELO1 (27) which could presumably elongate 16:0-CoA to 18:0-

CoA. This indicates that diatoms developed very different route of biosynthesis from plants, where the canonical conversion of 16:0 to 18:0 is carried out by plastidial a β-ketoacyl-ACP synthase II (KASII). Recently, Aslan et al., demonstrated that KO of KASII in tobacco resulted in increased accumulation of C16 FAs (28), suggesting that plants do not have an ability to utilize ER-located elongase for conversion of plastid 16:0 to 18:0. In the *P. tricornutum* genome a KASII orthologue has been annotated but not functionally characterized. Further modification of 18:0-CoA could be carried out by orthologues of the Arabidopsis ADS1, to produce 18:1Δ9-CoA. We identified only one putative Δ9-oleyl desaturase sequence, Phatr_28797, with an N-terminal sequence consistent with an ER localization. The present results suggest that acyl-CoA desaturase participates in desaturation at the Δ9 position of 18:0 in the ER. The role of two putative Δ0-elongases and Δ9-oleyl desaturase in LC-PUFA biosynthesis is under investigation.

In higher plants, *de novo* plastidial 16:0- and 18:0-ACPs can enter two distinct routes of lipid synthesis, the “prokaryotic” or “eukaryotic”. The “prokaryotic” or “eukaryotic” structure of plastid lipids is determined by the origin of phosphatidic acid (PA) and DAG. In plants, FA synthesized in the chloroplast are transferred onto glycerol-3-phosphate (G3P) by a plastidial acyl-G3P acyltransferase (ATS1). Further esterification by the plastid LPAAT, (ATS2), leads to the production of PA and DAG with C18 and C16 at position *sn*-1 and *sn*-2 respectively. Chloroplast desaturases acting on 16:0 produce a range of C16 unsaturated FA, found at the *sn*-2 position of MGDG and DGDG lipids. In the “eukaryotic” pathway, acyl-ACPs are hydrolysed by FAT to produce free FAs which are exported to the ER for the subsequent incorporation into membrane glycerolipids with C18 at *sn*-2 position before re-import to the chloroplast. The presence of a eukaryotic pathway involving recycling of diacylglycerol backbone coming from phospholipid for galactolipid synthesis, as described in higher plants, has not been demonstrated in Heterokonts. In *P. tricornutum*, EPA found in chloroplast lipids will have been synthesized in the ER by ER-located desaturases and elongases (17). Thus, EPA and other LC-PUFAs must also be re-imported to secondary plastids for incorporation into the plastidial glycolipids. However, the nature of precursors that are transported over the chloroplast-limiting membranes remains unknown.

In all analysed chloroplast lipids of WT and mutant cells EPA is exclusively found in the sn-1 position whereas C16 occupy mainly the *sn*-2 position, confirming the

observation that the prokaryotic pathway for the synthesis of the glycerolipids is dominant in Heterokonts (3, 29, 27). This also suggests that the plastid LPAAT has a very high selectivity for C16 fatty acids as the acyl donors to generate *sn*-2-C16- PA giving rise to lipids with the prokaryotic signature. ER membrane glycerolipids of WT and both mutants, such as PC, DGTA and PE mostly have C18, C20 and C22 FA together with C16 species esterified at the *sn*-2 position indicating that either microsomal LPAAT has no selectivity for FA species or acyl-CoA:lysophospholipid acyltransferase (LPCAT) may be involved in ER membrane glycerolipid assembly.

In the different *P. tricornutum* cells used in this study, TAGs are always enriched in C16 fatty acids at their *sn*-2 position implying that the TAG synthesis may be similar to that described in *Chlamydomonas reinhardtii* where a chlorophyte-specific acyltransferase, CrLPAAT2, localized to the ER, prefers 16:0-CoA as the substrate for synthesis of glycerolipid intermediates for TAG assembly and/or transfer to the plastid (30). Since C18 and C20 are hardly detected at the *sn*-2 position in thylakoid lipids in WT and OE cells, similar selectivity may operate in *P. tricornutum*, implying that ER-synthesized precursors (C16 bound to *sn*-2-PA) have diagnostic C16 acyl chains esterified at this position. A >20-fold increase in specific signature 20:5/16:0 form in DAG of KO cells followed by similar increase in this form in thylakoid lipids supports this hypothesis. Interestingly, MGDG and SQDG in KO cells contain increased levels of C18 bound to *sn*-2 molecular species concomitant with an increase in these forms (16:1/18:1; 20:5/18:1, 20:5/18:2) in PE, PC and DGTA suggesting a potential existence of a eukaryotic pathway with a recycling of a diacyl precursors coming from phospholipid for galactolipid synthesis, as described in higher plants and *C. reinhardtii* (31). Alternatively, ER located PA and DAG may serve as precursors of galactolipid and sulfolipid synthesis.

An increase of 16:1 and concomitant reduction in EPA levels in TAG in OE cells may indicate that *de novo* FA synthesis contributes to TAG biosynthesis via the Kennedy pathway involving a diacylglycerol acyltransferase and *de novo* DAG and acyl-CoA synthesis. This may be supported by the observed decrease in 16:1 and increase in EPA levels in KO cells. Despite the significant changes to the FA profile, OE or KO of the *PAD* gene does not significantly change the total FA accumulation relative to WT, indicating no change in *de novo* FA synthesis. In addition, the DAG acyl composition does not fully reflect the composition of the main membrane lipids in support of a *de novo* synthesis and, in contrast to plants, does not indicate any substantial recycling of DAG moieties deriving

from membrane glycerolipids (32). ER-synthesized EPA may be also imported into chloroplast and incorporated into glycolipids by the suggested “omega pathway”. Newly formed EPA may be released from a phospholipid into the cytosolic acyl-CoA pool and then transported into the chloroplasts to be attached to MDGD at the sn-1 position by the first acyltransferase, ATS1(19).

Conclusions

The role of EPA in chloroplast lipids remains unknown. Based on the observation that the turnover of EPA-rich MGDG is higher under NPQ-inducing conditions, Dolch et al 2017 (27) suggested that EPA could act as a sacrificial molecule acting as supramolecular antioxidant capturing oxygen species during light stress. The results of our light stress experiments do not support this hypothesis as the growth rates in OE cells with less EPA/more MGDG were not inhibited relative to the WT by light stress. However, the growth of KO cells containing more EPA /less MGDG was inhibited, probably indicating the presence of EPA in plastids is more important for membrane fluidity in cold adaptation. We propose that the PAD gene acts as a key factor in determining EPA levels to maintain phenotypic plasticity. In particular, the modulation of both MGDG and TAG levels through the presence/absence of 16:1n7 represents a simple “tag” by which different lipids can be sorted for further modification.

Materials and Methods

Strain and culture conditions. *P. tricornutum* Pt4 strain (*UTEX 646*) was grown in artificial sea water (Instant Ocean, Spectrum Brands) supplemented with F/2 nutrients. Cultures were grown at 20°C under constant illumination (100 µmols m^{-2} s^{-1}, 4000K White and 660nm LED lighting) and agitated continuously at 70 rpm. Growth was monitored by OD_{750nm} calibrated to cell density measured by an automated cell counter (Cellometer T4, Nexcelom). Lines were maintained on F/4 agar plates grown at 20°C under 50 µmols m^{-2} s^{-1} (3500K fluorescent tubes).

Construction of acyl-ACP Δ9-desaturase Overexpression Cassette and Transformation. The *PAD* (Phatr3_J9316) gene was chemically synthesised (Genscript, USA) and codon optimised to remove conflicting restriction sites. The PAD gene was

inserted into position 1 in the two-gene cassette transformation vector pPhOS2 (21) under the control of the EF2 promoter (22) generating pPhOS2_PAD construct. Construction of the transformation cassette pPhOS2_PAD is described in detail in *SI Appendix, SI Materials and Methods*. Transformation of P*. tricornutum* Pt4 via biolistic transformation and screening was carried as described previously (21).

Generation of acyl-ACP Δ9-desaturase KO lines. A universal knock-out CRISPR/Cas9 vector was constructed with a dual sgRNA design (33) using dual reporter gene selection system (designed by Mark Youles, personal communication). Type IIS LOOP DNA assembly was used for Level 1 and 2 vector constructions, following the method described in Pollak et al., 2018 (34). The design of KO cassettes is explained in detail in *SI Appendix, SI Materials and Methods*. Transformation of P*. tricornutum* Pt4 via biolistic transformation and screening was carried as described previously (21).

Cloning of acyl-ACP Δ9-desaturase (Phatr3_J9316) into *Synechocystis* expression vector and functional characterization in *Synechocystis*. To generate the Syn_PAD strain, the *Synechocystis* PCC6803 glucose-tolerant WT (Syn_WT, Himadri Pakrasi, Department of Biology, Washington University, St Louis, MO, USA) was transformed with the self-replicative vector pUR (35) expressing the acyl-ACP Δ9-desaturase gene lacking the 5' putative signal peptide sequence (as predicted by SignalP online software). Generation of the vector, transformation and functional characterisation of the Phatr3_J9316 gene is described in detail in *SI Appendix, SI Materials and Methods*.

RNA Extraction and qRT-PCR. For RNA extraction, 1-1.5x10^8 exponential phase cells were pelleted, flash frozen in liquid nitrogen and stored at -80°C. RNA extraction was carried out using the method described in Smith *et al.,* 2018 (36). cDNA was synthesised and q-PCR analysis was carried out as described detail in *SI Appendix, SI Materials and Methods*.

Lipid analysis. Whole biomass FAME analysis was carried out following as previously reported (21), using of pentadecanoic acid and tricosanoic acid internal standards. Further details are described in *SI Appendix, SI Materials and Methods*.

Glycerolipids were extracted following a method adapted from (29), further details are described in *SI Appendix, SI Materials and Methods*.

For positional analysis, lipids first were fractionated by 1D and 2D TLC (described in detail in *SI Appendix, SI Materials and Methods*), purified classes were then characterised by preferential loss analysis under low-energy collision-induced dissociation as described in previously described (3). After species characterisation, quantification of each species was carried out by LC-MS/MS as previously described (24).

Chlorophyll analysis. For chlorophyll analysis, 1.5-3x10^7 exponential phase cells were pelleted, washed in ammonium formate and frozen at -20°C. Chlorophyll was extracted with 2 ml of methanol and absorption was measured as outlined (37).

Transmission Electron Microscopy. TEM imaging was carried out by Rothamsted Bioimaging (Harpenden). Processing of *P. tricornutum* cells for TEM imaging is described in detail in the *SI Appendix, SI Materials and Methods*.

Statistics. One-way analysis of variance (ANOVA) was applied to data on specific growth, fatty acid, lipid class, and lipid species data. Data was transformed by natural log (quantitative data) or logit (relative %). Post-hoc comparison of the means was carried out using least significant difference (LSD) at 5%, 1% and 0.1% level of significance. A two-tailed Student's t-test was carried out in cases where only two strains are compared. Microsoft Excel was used for these analyses.

Acknowledgments

Rothamsted Research receives grant-aided support from the Biotechnology and Biological Sciences Research Council (BBSRC), UK and this project was supported by grant BB/L002957/1. We would like to thank the following: Prof. Annegret Wilde for providing the pUR vector and Prof. Dario Leister for providing the *Synechocystis* PCC6803 GT WT strain. Dr Katrin Geisler for providing cloning modules (Ble, FcpB promoter, FcpC terminator). Dr. Mark Youles for providing technical advice and pICSL002215 vector (containing mRFP gene). Dr Bernado Pollack for providing Loop assembly vectors. Prof. Per Winge for providing pKS_diacas9 vector. Dr Chloe Economou for technical assistance. Dr Rebecca Lauder for bioimaging.

Supplementary Figures

Fig. S1. Schematic map of the expression vector pPhOS2_ *PAD*.

Fig. S2. Selection of transgenic *P. tricornutum* lines overexpressing an acyl-ACP Δ9-desaturase.

Fig. S3. FA and glycerolipid classes comparison in the WT and overexpressor strains (PAD#16 and PAD#32) during the stationary stage (8 days).

Fig. S4. Identification of glycerolipids from *P. tricornutum*

Fig. S5. Generation of cloning cassettes for pRS Ble_DiaCas9_sgRNA2 and KO line analysis.

Fig. S6. Fatty acids and glycerolipid analysis of the WT and KO strains (Δ*pad*#3 and (Δ*pad*#7) during the stationary stage of growth phase (8 days).

Fig S7. Generation of transgenic SynDes9 strains**.**

Fig S8. Fatty acid composition (µg FA ml culture^{-1}) of Syn_WT and Syn_PAD strains.

Fig. S9. Transmission electron micrograph of WT and transgenic strains.

Fig. S10. Cellular growth of WT and transgenic strains.

Fig. S11. Chlorophyll content of WT and transgenic strains.

Fig. S12. Cellular growth of WT and transgenic strains under light stress.

Fig. S13. Proposed pathway for EPA biosynthesis in OE PAD cells.

Supplementary Tables

Table S1. The major molecular species for each lipid class in E phase PAD cells as relative (mol %) values.

Table S2. The major molecular species for each lipid class in E phase PAD in absolute amounts.

Table S3 The major molecular species for each lipid class in S phase PAD cells as relative (mol %) values.

Table S4. The major molecular species for each lipid class in PAD cells given in absolute amounts.

Table S5. The major molecular species for each lipid class in E phase Δpad cells as relative (mol %) values.

Table S6. The major molecular species for each lipid class in E phase Δpad cells given in absolute amounts

Table S7. The major molecular species for each lipid class in S phase Δpad cells as relative (mol %) values.

Table S8. The major molecular species for each lipid class in S phase Δpad cells in absolute amounts

Table S9. Fatty acid quantification in major lipid classes of S phase Δpad cells.

Table S10. Primers used in this study

References

1. J. Prihoda *et al.*, Chloroplast-mitochondria cross-talk in diatoms. *Journal of Experimental Botany* **63**, 1543-1557 (2012).
2. S. Flori, P. H. Jouneau, G. Finazzi, E. Marechal, D. Falconet, Ultrastructure of the Periplastidial Compartment of the Diatom Phaeodactylum tricornutum. *Protist* **167**, 254-267 (2016).
3. H. Abida *et al.*, Membrane Glycerolipid Remodeling Triggered by Nitrogen and Phosphorus Starvation in Phaeodactylum tricornutum. *Plant Physiology* **167**, 118-136 (2015).
4. J. Popko *et al.*, Metabolome Analysis Reveals Betaine Lipids as Major Source for Triglyceride Formation, and the Accumulation of Sedoheptulose during Nitrogen-Starvation of Phaeodactylum tricornutum. *Plos One* **11** (2016).
5. Y. Liang, Y. Maeda, T. Yoshino, M. Matsumoto, T. Tanaka, Profiling of Polar Lipids in Marine Oleaginous Diatom Fistulifera solaris JPCC DA0580: Prediction of the Potential Mechanism for Eicosapentaenoic Acid-Incorporation into Triacylglycerol. *Marine Drugs* **12**, 3218-3230 (2014).
6. I. A. Guschina, J. L. Harwood, Lipids and lipid metabolism in eukaryotic algae. *Progress in Lipid Research* **45**, 160-186 (2006).
7. J. Shanklin, J. E. Guy, G. Mishra, Y. Lindqvist, Desaturases: Emerging Models for Understanding Functional Diversification of Diiron-containing Enzymes. *Journal of Biological Chemistry* **284**, 18559-18563 (2009).
8. Y. Gong, X. Guo, X. Wan, Z. Liang, M. Jiang, Characterization of a novel thioesterase (PtTE) from Phaeodactylum tricornutum. *Journal of Basic Microbiology* **51**, 666-672 (2011).
9. J. A. Schnurr, J. M. Shockey, G. J. de Boer, J. A. Browse, Fatty acid export from the chloroplast. Molecular characterization of a major plastidial acyl-coenzyme A synthetase from Arabidopsis. *Plant Physiology* **129**, 1700-1709 (2002).
10. Y. Li-Beisson, J. J. Thelen, E. Fedosejevs, J. L. Harwood, The lipid biochemistry of eukaryotic algae. *Progress in Lipid Research* **74**, 31-68 (2019).
11. M. Fukuchi-Mizutani *et al.*, Characterization of Delta 9 acyl-lipid desaturase homologues from Arabidopsis thaliana. *Plant and Cell Physiology* **39**, 247-253 (1998).
12. C. Bowler *et al.*, The Phaeodactylum genome reveals the evolutionary history of diatom genomes. *Nature* **456**, 239-244 (2008).
13. K. E. Apt, P. G. Kroth-Pancic, A. R. Grossman, Stable nuclear transformation of the diatom Phaeodactylum tricornutum. *Mol Gen Genet* **252** (1996).
14. W. Yongmanitchai, O. P. Ward, MOLECULAR-SPECIES OF TRIACYLGLYCEROLS FROM THE FRESH-WATER DIATOM, PHAEODACTYLUM-TRICORNUTUM. *Phytochemistry* **32**, 1137-1139 (1993).
15. T. Arao, A. Kawaguchi, M. Yamada, POSITIONAL DISTRIBUTION OF FATTY-ACIDS IN LIPIDS OF THE MARINE DIATOM PHAEODACTYLUM-TRICORNUTUM. *Phytochemistry* **26**, 2573-2576 (1987).
16. T. Arao, T. Sakaki, M. Yamada, BIOSYNTHESIS OF POLYUNSATURATED LIPIDS IN THE DIATOM, PHAEODACTYLUM-TRICORNUTUM. *Phytochemistry* **36**, 629-635 (1994).

17. F. Domergue, J. Lerchl, U. Zahringer, E. Heinz, Cloning and functional characterization of Phaeodactylum tricornutum front-end desaturases involved in eicosapentaenoic acid biosynthesis. *European Journal of Biochemistry* **269**, 4105-4113 (2002).
18. F. Domergue *et al.*, New insight into Phaeodactylum tricornutum fatty acid metabolism. Cloning and functional characterization of plastidial and microsomal Delta 12-fatty acid desaturases. *Plant Physiology* **131**, 1648-1660 (2003).
19. D. Petroutsos *et al.*, Evolution of galactoglycerolipid biosynthetic pathways - From cyanobacteria to primary plastids and from primary to secondary plastids. *Progress in Lipid Research* **54**, 68-85 (2014).
20. L.-J. Dolch, E. Marechal, Inventory of Fatty Acid Desaturases in the Pennate Diatom Phaeodactylum tricornutum. *Marine Drugs* **13**, 1317-1339 (2015).
21. M. L. Hamilton, R. P. Haslam, J. A. Napier, O. Sayanova, Metabolic engineering of Phaeodactylum tricornutum for the enhanced accumulation of omega-3 long chain polyunsaturated fatty acids. *Metabolic Engineering* **22**, 3-9 (2014).
22. S. Seo, H. Jeon, S. Hwang, E. Jin, K. S. Chang, Development of a new constitutive expression system for the transformation of the diatom Phaeodactylum tricornutum. *Algal Research-Biomass Biofuels and Bioproducts* **11**, 50-54 (2015).
23. F. Domergue *et al.*, Acyl carriers used as substrates by the desaturases and elongases involved in very long-chain polyunsaturated fatty acids biosynthesis reconstituted in yeast. *Journal of Biological Chemistry* **278**, 35115-35126 (2003).
24. J. Jouhet *et al.*, LC-MS/MS versus TLC plus GC methods: Consistency of glycerolipid and fatty acid profiles in microalgae and higher plant cells and effect of a nitrogen starvation. *Plos One* **12** (2017).
25. W. Yongmanitchai, O. P. Ward, POSITIONAL DISTRIBUTION OF FATTY-ACIDS, AND MOLECULAR-SPECIES OF POLAR LIPIDS, IN THE DIATOM PHAEODACTYLUM-TRICORNUTUM. *Journal of General Microbiology* **139**, 465-472 (1993).
26. I. Heilmann, S. Mekhedov, B. King, J. Browse, J. Shanklin, Identification of the Arabidopsis palmitoyl-monogalactosyldiacylglycerol Delta 7-desaturase gene FAD5, and effects of plastidial retargeting of Arabidopsis desaturases on the fad5 mutant phenotype. *Plant Physiology* **136**, 4237-4245 (2004).
27. L. J. Dolch *et al.*, A Palmitic Acid Elongase Affects Eicosapentaenoic Acid and Plastidial Monogalactosyldiacylglycerol Levels in Nannochloropsis. *Plant Physiology* **173**, 742-759 (2017).
28. S. Aslan, P. Hofvander, P. Dutta, F. Sitbon, C. X. Sun, Transient silencing of the KASII genes is feasible in Nicotiana benthamiana for metabolic engineering of wax ester composition. *Scientific Reports* **5** (2015).
29. D. Simionato *et al.*, The Response of Nannochloropsis gaditana to Nitrogen Starvation Includes De Novo Biosynthesis of Triacylglycerols, a Decrease of Chloroplast Galactolipids, and Reorganization of the Photosynthetic Apparatus. *Eukaryotic Cell* **12**, 665-676 (2013).
30. J. Kim *et al.*, Flux balance analysis of primary metabolism in the diatom Phaeodactylum tricornutum. *Plant Journal* **85**, 161-176 (2016).
31. J. L. Fan, C. Andre, C. C. Xu, A chloroplast pathway for the de novo biosynthesis of triacylglycerol in Chlamydomonas reinhardtii (vol 585, pg 1985, 2011). *Febs Letters* **585**, 4029-4029 (2011).

32. P. D. Bates, J. Browse, The significance of different diacylgycerol synthesis pathways on plant oil composition and bioengineering. *Frontiers in Plant Science* **3** (2012).
33. Y. F. Mao *et al.*, Application of the CRISPRCas System for Efficient Genome Engineering in Plants. *Molecular Plant* **6**, 2008-2011 (2013).
34. B. Pollak *et al.*, Loop assembly: a simple and open system for recursive fabrication of DNA circuits. *New Phytologist* **222**, 628-640 (2019).
35. A. Wiegard *et al.*, Biochemical analysis of three putative KaiC clock proteins from Synechocystis sp PCC 6803 suggests their functional divergence. *Microbiology-Sgm* **159**, 948-958 (2013).
36. S. R. Smith, R. M. Abbriano, M. Hildebrand, Comparative analysis of diatom genomes reveals substantial differences in the organization of carbon partitioning pathways. *Algal Research-Biomass Biofuels and Bioproducts* **1**, 2-16 (2012).
37. R. J. Ritchie, Universal chlorophyll equations for estimating chlorophylls a, b, c, and d and total chlorophylls in natural assemblages of photosynthetic organisms using acetone, methanol, or ethanol solvents. *Photosynthetica* **46**, 115-126 (2008).

Figures Legends

Figure 1. Analysis of FA and glycerolipids in transgenic *P. tricornutum* overexpressing acyl-ACP Δ9 desaturase. (*A*) Quantitative analysis of FA composition in total lipids (µg FA 10^6 cells^{-1}) in WT and transgenic PAD lines during E phase. (*B*) Glycerolipid classes comparison from WT and transgenic PAD lines during the E phase of growth (3 days). Insert: Quantitative analysis of total glycerolipids (nmol of lipid 10^6 cells^{-1}). Values expressed are relative % of total lipids Growth stage was determined by analysing cell density. Values presented are the average of three biological replicates, error bars represent SE. Asterisks indicate significant difference ($p<0.05$, LSD) relative to WT.

Figure 2. Generation of acyl-ACP Δ9 desaturase KO strains by CRISPR/Cas9. (*A*) Schematic structure (important features) of the CRISPR/Cas9 target locus within the Δ9 desaturase gene. The positions of guide RNA complimentary binding sites in the first exon are indicated with black arrows. The approximate region of nucleotide deletion is shown in white. The grey arrows indicate the site of amplification for PCR genotyping and qPCR of cDNA. (*B*) PCR screen of native acyl-ACP Δ9 desaturase gene in KO lines (see *SI Appendix,* (Fig. S5) for position of primers and expected deletion). Single band shift indicates bi-allelic deletion. (*C*) Transcript abundance of acyl-ACP Δ9 desaturase (Phatr3_J9316) and putative Δ9 acyl-CoA desaturase, ADS (Phatr3_J28797) genes. Expression is reported relative to the reference gene Aureochrome (Phatr3_J8113). Values presented are the average of three biological replicates, error bars represent SE. Asterisks indicate significant difference relative to WT ($p<0.05$, LSD).

Figure 3. FA and glycerolipid classes comparison in the WT and KO strains during the exponential stage of growth phase (3 days). (*A*) FA content. Values expressed in µg FA 10^6 cells^{-1}. (*B*) Glycerolipid classes. Values expressed in % of total lipids. Insert: Quantitative analysis of total glycerolipids (nmol of lipid 10^6 cells^{-1}). Growth stage was determined by analysing cell density. Values presented are the average of three biological replicates, error bars represent SE. Asterisks indicate significant difference relative to WT ($p<0.05$, LSD).

Figure 4. Proposed pathway for EPA biosynthesis and possible EPA import routes from the ER into the chloroplast of *P. tricornutum*. Red text indicates increased pool size of metabolite or activity of enzyme in KO cells. Blue text indicates reduced pool size

or activity of enzyme. *De novo* synthesized 16:0-ACP enters prokaryotic pathway where it can be used in the plastid for the production of MGDG, DGDG, SQDG, and PG via a canonical prokaryotic pathway or desaturated by PAD to 16:1n7-ACP and further by soluble ACP desaturases. When exported to the cytosol through the LACS pathway to enter eukaryotic pathway, C16-ACPs are first hydrolysed by unknown FAT and FFA are exported through the plastidial membrane to enter CoA pool. 16:0-CoA in elongated to 18:0-CoA with further desaturation by homologue of Arabidopsis ADS1, Δ9-acyl-CoA desaturase to produce 18:1Δ9-CoA which is at the base of PUFA biosynthesis. Newly produced EPA could be incorporated into acyl-CoA and imported from ER into the chloroplast for galactolipid synthesis. From the ER EPA could be imported into chloroplast as incorporated into PA or DAG. EPA can be converted into TAG by an acyl-independent PDAT after acyl-editing or enter the Kennedy pathway and be converted into TAG by DGAT. ATS1, plastidic glycerol-3-phosphate acyltransferase; ATS2, plastidic lysophosphatidic acid transferase; PGPS, phosphatidylglycerol phosphate synthase; SQD2, SQDG synthase 2; MGD, MGDG synthase; DGD, DGDG synthase.

Figures

A

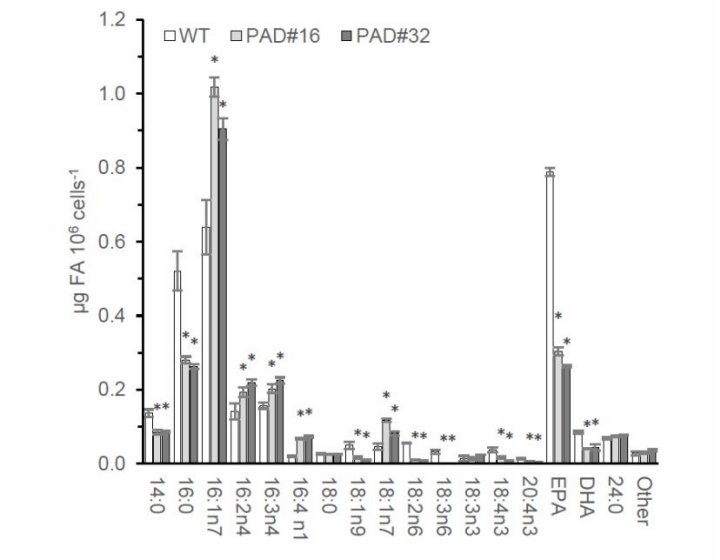

B

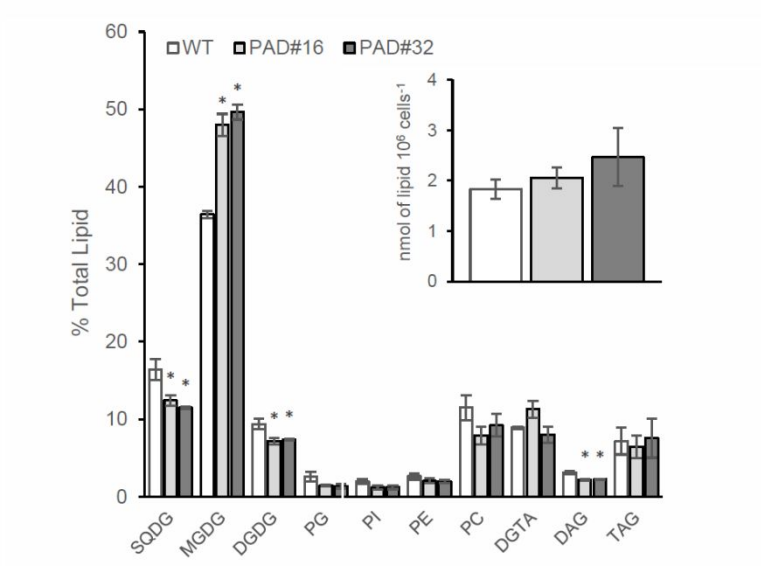

Figure 1. Analysis of FA and glycerolipids in transgenic *P. tricornutum* overexpressing acyl-ACP Δ9 desaturase. (*A*) Quantitative analysis of FA composition in total lipids (µg FA 10^6 cells^{-1}) in WT and transgenic PAD lines during E phase. (*B*) Glycerolipid classes comparison from WT and transgenic PAD lines during the E phase of growth (3 days). Insert: Quantitative analysis of total

glycerolipids (nmol of lipid 10^6 cells^{-1}). Values expressed are relative % of total lipids Growth stage was determined by analysing cell density. Values presented are the average of three biological replicates, error bars represent SE. Asterisks indicate significant difference ($p<0.05$, LSD) relative to WT.

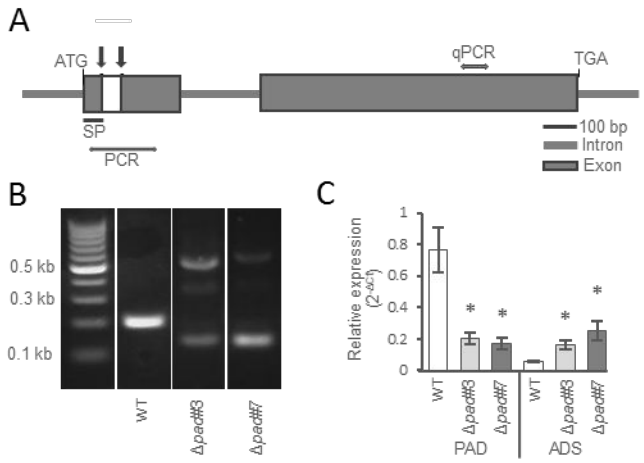

Figure 2. Generation of acyl-ACP Δ9 desaturase KO strains by CRISPR/Cas9. (*A*) Schematic structure (important features) of the CRISPR/Cas9 target locus within the Δ9 desaturase gene. The positions of guide RNA complimentary binding sites in the first exon are indicated with black arrows. The approximate region of nucleotide deletion is shown in white. The grey arrows indicate the site of amplification for PCR genotyping and qPCR of cDNA. (*B*) PCR screen of native acyl-ACP Δ9 desaturase gene in KO lines (see *SI Appendix,* (Fig. S5) for position of primers and expected deletion). Single band shift indicates bi-allelic deletion. (*C*) Transcript abundance of acyl-ACP Δ9 desaturase (Phatr3_J9316) and putative Δ9 acyl-CoA desaturase, ADS (Phatr3_J28797) genes. Expression is reported relative to the reference gene Aureochrome (Phatr3_J8113). Values presented are the average of three biological replicates, error bars represent SE. Asterisks indicate significant difference relative to WT ($p<0.05$, LSD).

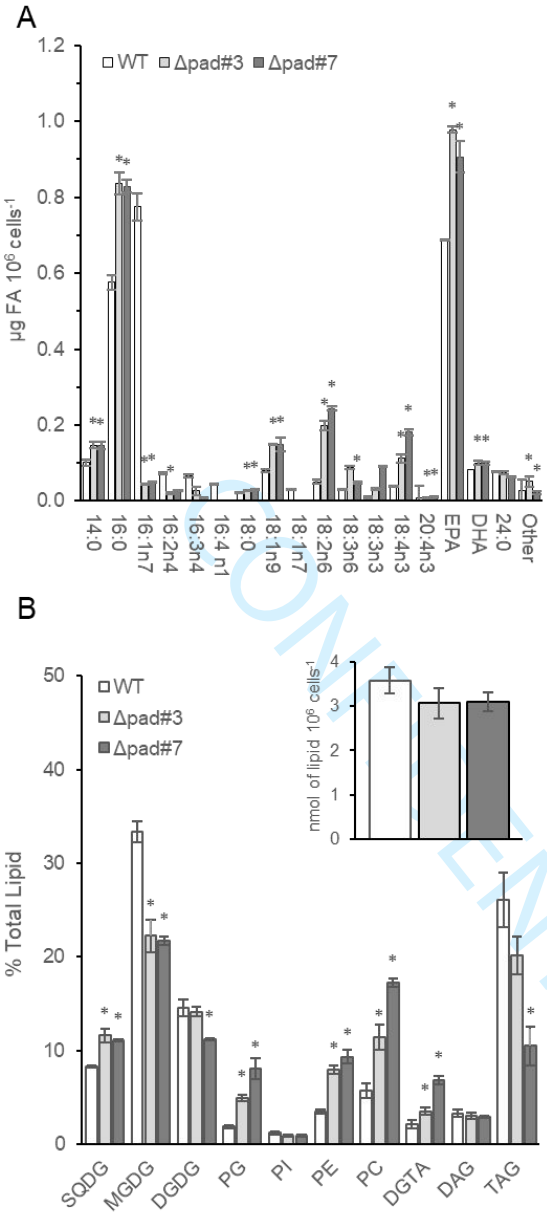

Figure 3. FA and glycerolipid classes comparison in the WT and KO strains during the exponential stage of growth phase (3 days). (*A*) FA content. Values expressed in µg FA 10^6 cells^{-1}. (*B*) Glycerolipid classes. Values expressed in % of total lipids. Insert: Quantitative analysis of total glycerolipids (nmol of lipid 10^6 cells^{-1}). Growth stage was determined by analysing cell density. Values presented are the average of three biological replicates, error bars represent SE. Asterisks indicate significant difference relative to WT ($p<0.05$, LSD).

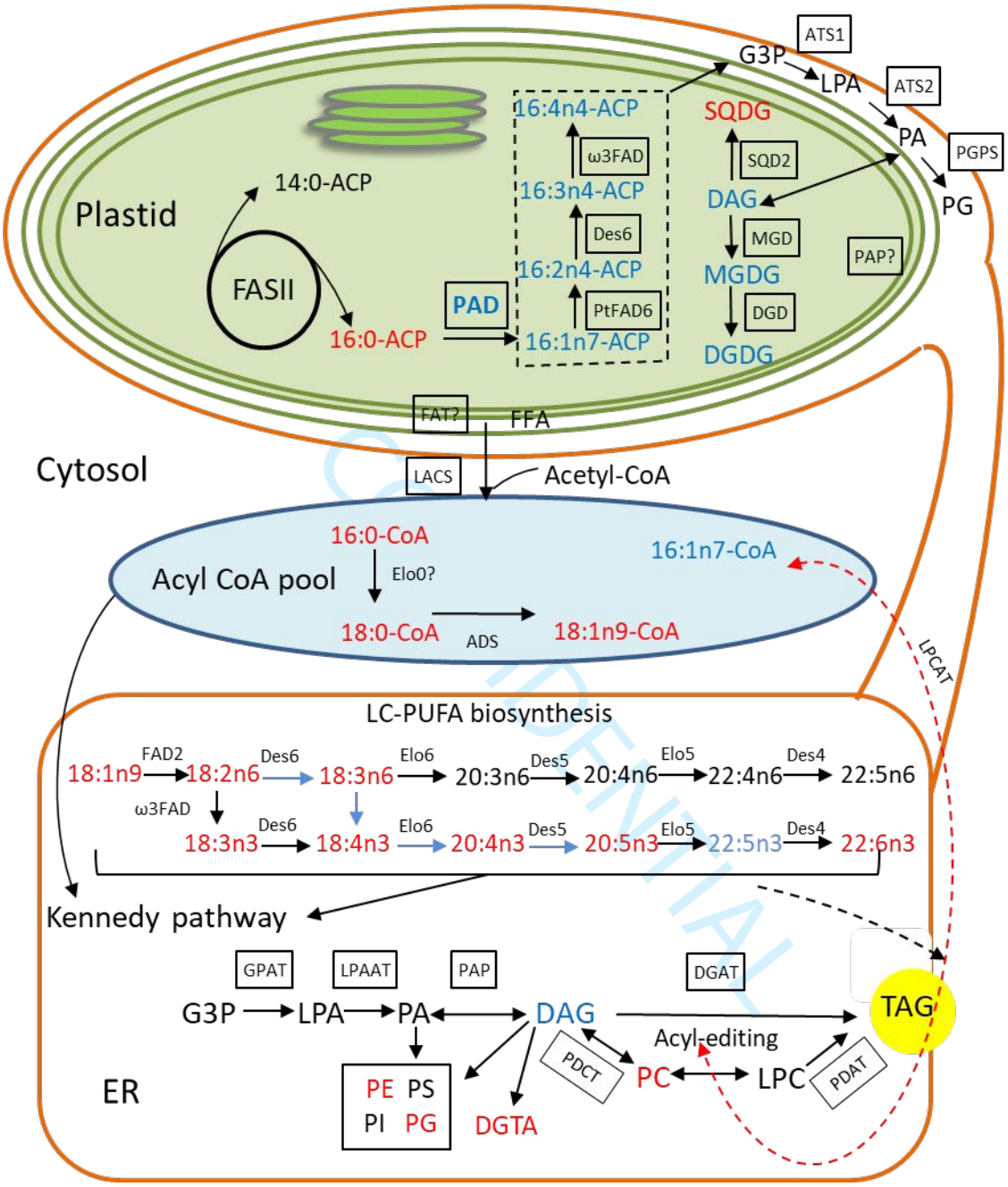

Figure 4. Proposed pathway for EPA biosynthesis and possible EPA import routes from the ER into the chloroplast of *P. tricornutum*. Red text indicates increased pool size of metabolite or activity of enzyme in KO cells. Blue text indicates reduced pool size or activity of enzyme. *De novo* synthesized 16:0-ACP enters prokaryotic pathway where it can be used in the plastid for the production of MGDG, DGDG, SQDG, and PG via a canonical prokaryotic pathway or desaturated by PAD to 16:1n7-ACP and further by soluble ACP desaturases. When exported

to the cytosol through the LACS pathway to enter eukaryotic pathway, C16-ACPs are first hydrolysed by unknown FAT and FFA are exported through the plastidial membrane to enter CoA pool. 16:0-CoA in elongated to 18:0-CoA with further desaturation by homologue of Arabidopsis ADS1, Δ9-acyl-CoA desaturase to produce 18:1Δ9-CoA which is at the base of PUFA biosynthesis. Newly produced EPA could be incorporated into acyl-CoA and imported from ER into the chloroplast for galactolipid synthesis. From the ER EPA could be imported into chloroplast as incorporated into PA or DAG. EPA can be converted into TAG by an acyl-independent PDAT after acyl-editing or enter the Kennedy pathway and be converted into TAG by DGAT. ATS1, plastidic glycerol-3-phosphate acyltransferase; ATS2, plastidic lysophosphatidic acid transferase; PGPS, phosphatidylglycerol phosphate synthase; SQD2, SQDG synthase 2; MGD, MGDG synthase; DGD, DGDG synthase.